

THE SOLAR NEIGHBORHOOD. XIV. PARALLAXES FROM THE CERRO TOLOLO INTER-AMERICAN OBSERVATORY PARALLAX INVESTIGATION—FIRST RESULTS FROM THE 1.5 m TELESCOPE PROGRAM

EDGARDO COSTA¹ AND RENÉ A. MÉNDEZ¹

Departamento de Astronomía, Universidad de Chile, Casilla 36-D, Santiago, Chile; costa@das.uchile.cl, rmendez@das.uchile.cl

W.-C. JAO,¹ TODD J. HENRY,¹ JOHN P. SUBASAVAGE,¹ AND MISTY A. BROWN¹
Georgia State University, Atlanta, GA 30302-4106; jao@chara.gsu.edu, thenry@chara.gsu.edu,
subasavage@chara.gsu.edu, brown@chara.gsu.edu

AND

PHILIP A. IANNA¹ AND JENNIFER BARTLETT¹

University of Virginia, Charlottesville, VA 22903; pai@virginia.edu, jlb2j@virginia.edu

Received 2004 December 21; accepted 2005 March 23

ABSTRACT

Trigonometric parallaxes, proper motions, and $V_j(RI)_{KC}$ photometry are presented for 31 stars targeted by the Cerro Tololo Inter-American Observatory Parallax Investigation (CTIOPI), a program of wide scope aimed at discovering and characterizing nearby stars. The data given are the first that have been obtained with the CTIO 1.5 m telescope, targeting a fainter subset of the CTIOPI input list. We present the first trigonometric parallaxes for 21 systems, of which one is within 10 pc (LP 647-013 at 9.59 ± 0.22 pc) and six are between 10 and 25 pc. Concurrently with our Cerro Tololo 0.9 m program, we have determined parallaxes for DEN 1048–3956 and LTT 6933 that place them at 4.00 ± 0.03 and 16.24 ± 0.43 pc from the Sun, respectively. We also present an improved parallax for the important nearby triple system GJ 2005ABC, placing it at 7.72 ± 0.15 pc from the Sun. The remaining seven parallaxes are for calibration stars, whose values indicate that our results agree well with other parallax determinations. We present color-magnitude and color-color diagrams that, in combination with theoretical isochrones from the literature and other derived properties of the observed sample, have aided the identification of the general nature of each of our targets. We have in this way discovered five new subdwarfs and several very low mass stars, a few of which may be brown dwarfs.

Key words: astrometry — solar neighborhood — stars: distances — stars: general

1. INTRODUCTION

The nearest stars, being the brightest examples of their types, provide astronomers with much of our understanding of stellar astronomy. For most types of stars, the fundamental framework of stellar astronomy is built on direct measurements of luminosities, colors, temperatures, and masses of stars in the solar neighborhood. By investigating the luminosity function, mass function, kinematics, and multiplicity of stars in the solar vicinity, we can probe the stellar populations of the Galaxy, determine their contributions to its total mass, and estimate the age of the Galactic disk. Furthermore, a more complete census of the solar neighborhood (including precise distance determinations) is highly desirable for upcoming space-based planetary searches that will require well-constrained target lists.

Full comprehension of the overall significance of nearby star studies to astronomy led first to the creation in 1994 of the Research Consortium on Nearby Stars (RECONS),² a program of wide scope aimed at completing the census and understanding the nature, both individually and as a group, of the stellar sample within 10 pc. Then, in 1998, the Nearby Stars Research Project (NStars) was started, with its primary goals being to foster research on nearby stars and to produce a master database of stars in the solar neighborhood to a distance horizon of 25 pc.

Potential applications of the nearest stars are, however, hampered by the fact that the faint members of the solar neighborhood are significantly underrepresented. By 1997, the RECONS list of stars closer than 10 pc indicated that, assuming that the density of stellar systems within 5 pc carried out to 10 pc, 130 systems ($\sim 35\%$) were missing from the 10 pc census (Henry et al. 1997). The problem is worse to 25 pc, a distance at which the incompleteness is anticipated to be $\sim 60\%$ for the entire sky and nearly 70% for the southern sky (Henry et al. 2002).

Only large trigonometric parallax programs can help remedy this problem, so RECONS started the Cerro Tololo Inter-American Observatory Parallax Investigation (CTIOPI) in 1999, a 3 yr trigonometric parallax program aimed at discovering some 150 new southern star systems within 25 pc, thereby increasing the population of stars known within that distance by $\sim 20\%$. This survey was carried out at CTIO in Chile, under support of the NOAO Surveys Program,³ supplemented with Chilean time.

2. SAMPLE

To make our survey efficient at discovering truly close stars, our input target list was refined as much as possible, selecting candidate nearby stars on the basis of “closeness” indicators such as large proper motions and/or a photometric or spectroscopic

¹ Visiting Astronomer, CTIO. CTIO is operated by the Association of Universities for Research in Astronomy (AURA), Inc., under contract to the NSF.

² See <http://www.chara.gsu.edu/RECONS>.

³ See <http://www.noao.edu/gateway/surveys>.

TABLE 1
IDENTIFICATION OF THE TARGETS

ID	Name	R.A. (J2000.0)	Decl. (J2000.0)	Other Common Name	Spectral Type, Notes
1.....	GJ 2005ABC	00 24 44.19	-27 08 24.2	LHS 1070	M6.0 V, flare star
2.....	LHS 132	01 02 51.05	-37 37 43.7	LP 938-071	M7.5 V
3.....	LP 647-013	01 09 51.20	-03 43 26.4		M9.5 V
4.....	LHS 148	01 53 09.00	-33 25 02.1	LP 940-037	M0.0 VI
5.....	WT 84	02 17 28.45	-59 22 43.7	APMPM J0217-5923	M5.5 V
6.....	LHS 162	02 56 13.21	-35 08 26.9	LP 942-066	M1.0 VI
7.....	LP 412-031	03 20 59.70	+18 54 22.8		M8.0 V
8.....	WT 133	04 02 13.92	-43 25 26.6	APMPM J0402-4325	M4.5 V
9.....	APMPM J0425-7243	04 24 33.59	-72 43 05.1		M5.0 V
10.....	APMPM J0452-5819	04 51 37.34	-58 18 52.1		M6.5 V
11.....	LHS 1777	05 42 12.71	-05 27 55.6	GJ 2045	M5.0 V
12.....	GI 223.2	05 55 09.53	-04 10 07.1	G099-044	DZ9, WD
13.....	CE 426-023	06 22 44.96	-28 16 52.9		M4.5 V
14.....	WT 214	07 28 40.11	-61 20 41.4		M4.0 V
15.....	GI 283B	07 40 19.36	-17 24 46.0	L745-46B	M6.5 V
16.....	GI 283A	07 40 20.78	-17 24 49.2	L745-46A	DZQ6, WD
17.....	WT 233	07 56 13.42	-67 05 20.6		M0.0 VI
18.....	LHS 2065	08 53 36.17	-03 29 32.3		M9.5 V, flare star
19.....	DEN 1048-3956	10 48 14.56	-39 56 06.9		M8.0 V
20.....	CE 440-064	11 48 50.55	-28 33 23.0		M5.0 V
21.....	LHS 367	14 18 20.40	-52 24 12.6	LTT 5622	K8 VI
22.....	LHS 3003	14 56 38.25	-28 09 48.7		M5.0 V, flare star
23.....	SPM 57600401	16 13 17.19	-25 38 13.9		M4.0 V
24.....	GI 644C	16 55 35.25	-08 23 40.7	LHS 429	M6.5 V, flare star
25.....	LTT 6933	17 28 07.33	-62 27 14.3	GJ 1218	M4.0 V
26.....	LHS 3346	17 58 49.95	-56 05 41.5	L205-56	M4.0 V
27.....	WT 2180	19 48 22.66	-08 22 52.2		M5.5 V
28.....	APMPM J1957-4216	19 56 57.60	-42 16 23.0		M5.5 V
29.....	LTT 7944	20 07 15.37	-54 21 48.9		M3.0 V
30.....	LHS 3566	20 39 23.82	-29 26 34.7	LP 927-032	M6.0 V
31.....	APMPM J2204-3348	22 04 02.29	-33 47 38.9		M2.0 VI

NOTES.—The epoch of the coordinates is 2000.0. Units of right ascension are hours, minutes, and seconds, and units of declination are degrees, arcminutes, and arcseconds.

estimate of their distances. For example, six of the program stars reported here have $\mu > 1'' \text{ yr}^{-1}$ (our so-called MOTION sample, as described in Jao et al. 2005, hereafter J05), an important sample for the discovery of very nearby stars and high-velocity subdwarfs.

Our targets were then discriminated essentially on the basis of their apparent brightness and two working lists were produced; a bright sample ($V \sim 10-15$) to be observed with the CTIO 0.9 m telescope and a fainter ($V \sim 15-20$) sample to be observed with the CTIO 1.5 m telescope. The first final results from the 0.9 m effort (hereafter the 0.9 m CTIOPI) were published in J05. Here we present the first final trigonometric parallaxes and proper motions resulting from observations carried out with the 1.5 m telescope (hereafter the 1.5 m CTIOPI).

Table 1 gives the J2000.0 coordinates of the targets and information to aid in their identification, such as another common name and spectral types. The coordinates were extracted from Two Micron All Sky Survey (2MASS) scans obtained at an epoch similar to that of our parallax observations. For comparison purposes, however, the coordinates have been transformed to epoch 2000.0, using the proper motions obtained in the present investigation (see Table 2). With the exception of LHS 367, the spectral types presented in Table 1 are unpublished classifications obtained by G. Lo Curto et al. (2005, in preparation, hereafter L05) as a result of spectroscopic follow-

up observations being carried out with the ESO 3.5 m New Technology Telescope (see below). The spectral type for LHS 367 is from the unpublished classification given by RECONS (T. Beaulieu et al. 2005, in preparation, hereafter B05) based on CTIO data.

Finding charts for our targets are given on the RECONS Web site. They were made from images taken in the present survey, thereby showing the position of the program stars at a fairly recent epoch. The finders are $8''.2$ on a side; north is at the top, and east to the left. They have not been trimmed or centered on the program objects and therefore show exactly how the parallax frames were taken and how the reference system was defined (see § 3). The red circles indicate the parallax investigation targets and the green circles indicate the reference stars used in the final reduction.

Follow-up photometric and spectroscopic observations, necessary to determine accurate optical luminosities and fully characterize the nearby stars discovered, were started more or less simultaneously, using facilities at CTIO, La Silla (ESO), and Las Campanas Observatory (LCO). Here we also present the pertinent photometric data, but the spectroscopy will be published elsewhere (L05) once those observations are completed. We would like to point out that a few of the spectral types given in Table 1 (namely, those for LHS 2065, DEN 1048-3956, LHS 3003, and GI 644C) are slightly discrepant with those

TABLE 2
PARALLAX INVESTIGATION RESULTS

Name (1)	π_{rel} (mas) (2)	π_{corr} (mas) (3)	π_{abs} (mas) (4)	μ (arcsec yr ⁻¹) (5)	P.A. (deg) (6)	N_{fr} (7)	T (yr) (8)	N_{run} (9)	N_{ref} (10)	Filter (11)
Program Stars										
GJ 2005ABC.....	129.13 ± 2.48	0.34 ± 0.08	129.47 ± 2.48	0.6537 ± 0.0030	348.3 ± 0.44	36	2.3	7	13	<i>V</i>
LHS 132.....	81.75 ± 2.73	0.20 ± 0.06	81.95 ± 2.73	1.4791 ± 0.0025	79.8 ± 0.16	31	3.2	9	15	<i>R</i>
LP 647-013.....	103.36 ± 2.29	0.87 ± 0.09	104.23 ± 2.29	0.3607 ± 0.0018	87.1 ± 0.39	30	3.2	8	18	<i>I</i>
LHS 148.....	12.80 ± 2.87	1.35 ± 0.26	14.15 ± 2.88	1.0676 ± 0.0030	84.4 ± 0.25	27	3.3	6	11	<i>I</i>
WT 84.....	75.89 ± 3.02	0.72 ± 0.09	76.61 ± 3.02	0.5323 ± 0.0018	209.6 ± 0.38	32	2.9	7	12	<i>R</i>
LHS 162.....	11.69 ± 2.59	1.47 ± 0.09	13.16 ± 2.59	1.0165 ± 0.0019	137.7 ± 0.21	33	2.0	6	12	<i>R</i>
LP 412-031.....	63.97 ± 3.21	1.76 ± 0.70	65.73 ± 3.29	0.4257 ± 0.0017	125.6 ± 0.44	33	3.1	7	15	<i>I</i>
WT 133.....	30.70 ± 2.13	1.31 ± 0.08	32.01 ± 2.13	0.5803 ± 0.0014	176.5 ± 0.21	35	3.1	6	11	<i>I</i>
APMPM J0425-7243.....	16.99 ± 3.03	1.27 ± 0.12	18.26 ± 3.03	0.5122 ± 0.0028	31.2 ± 0.61	52	2.3	7	13	<i>I</i>
APMPM J0452-5819.....	56.98 ± 1.17	1.07 ± 0.05	58.05 ± 1.17	0.7213 ± 0.0009	193.6 ± 0.12	62	3.1	7	16	<i>I</i>
CE 426-023.....	19.02 ± 1.80	1.07 ± 0.12	20.09 ± 1.80	0.2064 ± 0.0018	215.3 ± 1.01	36	2.7	6	19	<i>I</i>
WT 214.....	31.39 ± 2.59	0.82 ± 0.11	32.21 ± 2.59	0.6275 ± 0.0019	316.5 ± 0.36	30	2.2	6	20	<i>R</i>
WT 233.....	10.43 ± 1.90	0.58 ± 0.05	11.01 ± 1.90	0.7585 ± 0.0021	317.3 ± 0.31	34	2.2	8	21	<i>R</i>
DEN 1048-3956.....	48.37 ± 1.81	1.41 ± 0.11	249.78 ± 1.81	1.5388 ± 0.0031	229.8 ± 0.23	26	1.3	4	19	<i>I</i>
CE 440-064.....	24.21 ± 1.49	0.90 ± 0.06	25.11 ± 1.49	0.6726 ± 0.0014	261.8 ± 0.20	37	2.4	8	18	<i>I</i>
LHS 367.....	17.22 ± 2.43	2.51 ± 0.24	19.73 ± 2.44	1.1400 ± 0.0037	249.4 ± 0.30	47	1.4	5	17	<i>V</i>
SPM 57600401.....	33.85 ± 4.97	0.85 ± 0.10	34.70 ± 4.97	0.3713 ± 0.0052	81.7 ± 1.30	30	2.1	5	20	<i>R</i>
LTT 6933.....	58.38 ± 1.61	3.18 ± 0.22	61.56 ± 1.62	0.9768 ± 0.0016	196.9 ± 0.16	52	2.0	5	18	<i>V</i>
LHS 3346.....	20.23 ± 1.49	1.41 ± 0.14	21.64 ± 1.50	0.7104 ± 0.0022	209.7 ± 0.32	42	1.3	5	22	<i>R</i>
WT 2180.....	51.78 ± 2.24	1.98 ± 0.18	53.76 ± 2.25	0.5505 ± 0.0020	231.2 ± 0.42	49	3.0	8	20	<i>I</i>
APMPM J1957-4216.....	28.44 ± 2.06	0.82 ± 0.13	29.26 ± 2.06	1.0266 ± 0.0018	171.5 ± 0.15	37	2.9	8	22	<i>I</i>
LTT 7944.....	30.68 ± 5.27	0.52 ± 0.06	31.20 ± 5.27	0.5656 ± 0.0129	161.2 ± 2.31	28	1.2	5	18	<i>R</i>
LHS 3566.....	56.38 ± 2.68	0.88 ± 0.07	57.26 ± 2.68	0.7994 ± 0.0023	157.6 ± 0.30	25	2.3	6	17	<i>I</i>
APMPM J2204-3348.....	15.99 ± 4.01	1.07 ± 0.17	17.06 ± 4.01	0.9792 ± 0.0029	151.7 ± 0.32	38	3.2	8	17	<i>I</i>
Calibration Stars										
LHS 1777.....	78.34 ± 2.33	1.77 ± 0.19	80.11 ± 2.34	0.9687 ± 0.0026	349.8 ± 0.25	30	2.2	4	18	<i>R</i>
GI 223.2.....	154.95 ± 2.66	1.98 ± 0.25	16.93 ± 2.67	2.3680 ± 0.0027	167.1 ± 0.11	35	2.2	8	17	<i>V</i>
GI 283B.....	105.81 ± 1.63	1.20 ± 0.09	107.01 ± 1.63	1.2706 ± 0.0016	115.8 ± 0.13	39	2.9	8	21	<i>I</i>
GI 283A.....	106.56 ± 1.62	1.20 ± 0.09	107.76 ± 1.62	1.2613 ± 0.0016	116.3 ± 0.13	39	2.9	8	21	<i>I</i>
LHS 2065.....	112.82 ± 2.03	0.51 ± 0.04	113.33 ± 2.03	0.5529 ± 0.0020	248.4 ± 0.38	25	3.1	7	18	<i>I</i>
LHS 3003.....	142.37 ± 3.21	2.93 ± 0.52	145.30 ± 3.25	0.9753 ± 0.0021	209.8 ± 0.25	50	2.5	9	18	<i>I</i>
GI 644C.....	152.90 ± 1.27	2.53 ± 0.39	155.43 ± 1.33	1.1872 ± 0.0012	222.9 ± 0.11	63	2.9	9	19	<i>I</i>

presented by Henry et al. (2004). It is possible that they could change somewhat after the final analysis.

3. THE ASTROMETRY

3.1. Observations

The astrometric observations were all carried out with the same Tektronix 2048 × 2048 detector (24 μm pixels) attached to the Cassegrain focus of the CTIO 1.5 m telescope in its f/13.5 configuration. This combination gives a nominal scale and field of 0".24 pixel⁻¹ and 8'.19 × 8'.19, respectively. The exact scale used in all our reductions was 0".2408 pixel⁻¹, which was determined empirically using the procedure described in Jao et al. (2003).

Although the 1.5 m telescope CCD controller (Arcon) had the ability to read out the chip using more than one of the four working amplifiers of the Tektronix CCD, only one amplifier was used for readout. This choice was motivated by the suspicion that by using multiple amplifiers the astrometric precision could be degraded. This configuration resulted in a read-out time in excess of 3 minutes. Gain and read noise were 2.2 e⁻ ADU⁻¹ and 3.8 e⁻, respectively. Analog-to-digital converter saturation occurred at

65,535 ADUs, prior to entering the CCD nonlinear region and before full well was reached.⁴

Before initiating the specific parallax observations of each program object ("pi star"), the fields around each of them were explored to establish a preliminary (see § 3.2) parallax reference frame. The preliminary reference frame was selected aiming to achieve a homogeneous distribution of reference stars of similar brightness around the pi star. The exploration was carried out in the *V*, *R*, and *I* bandpasses to determine in which filter the brightness of the field stars was comparable to the brightness of the pi star. Once the best bandpass was selected for a given target, the same filter was used throughout the program.

In general, the parallax targets were placed more or less near the center of the chip, but there were cases in which it was necessary to offset the pi star in order to come close to a spatially balanced distribution of reference stars. Once the positioning of a pi star on the chip was decided, all subsequent observations were made placing it within a few pixels of the chosen position. Apart from ensuring that all potential reference stars would be present in all images, this positioning strategy had the added

⁴ See <http://www.ctio.noao.edu/cfccd/cfccd.html>; § 4.1.

TABLE 3
COMPARISON WITH PUBLISHED TRIGONOMETRIC PARALLAXES AND PROPER MOTIONS

NAME	OUR RESULTS			PUBLISHED RESULTS			NOTES
	$\bar{\pi}_{\text{abs}}$ (mas)	μ (arcsec yr ⁻¹)	P.A. (deg)	$\bar{\pi}_{\text{abs}}$ (mas)	μ (arcsec yr ⁻¹)	P.A. (deg)	
Calibration Stars							
LHS 1777.....	80.11 ± 2.34	0.9687	349.8	78.2 ± 2.7	0.971	352	YPC 1310.01
				78.2 ± 2.7	0.9732	351.1	USNO ^a
				79.72 ± 1.89	0.9590	351.2	0.9 m CTIOPI
GI 223.2.....	156.93 ± 2.67	2.3680	167.1	155.0 ± 2.1	2.377	167	YPC 1363.02
GI 283A.....	107.76 ± 1.62	1.2613	116.3	112.4 ± 2.7	1.253	117	YPC 1813.00A
GI 283B.....	107.01 ± 1.63	1.2706	115.8	...	1.253	117	YPC 1813.00B; no parallax data
LHS 2065.....	113.33 ± 2.03	0.5529	248.4	117.3 ± 1.5	0.576	250	YPC 2122.01
LHS 3003.....	145.30 ± 3.25	0.9753	209.8	156.3 ± 3.0	0.965	210	YPC 3372.03
				159.2 ± 5.1	Tinney (1996)
GI 644C.....	155.43 ± 1.33	1.1872	222.9	No data for component C
				154.8 ± 0.6	1.183	223	YPC 3845.00 (components ABD)
				155.63 ± 1.81	1.2096	223.3	HIP 82817 (components ABD)
				169.8 ± 6.6	1.190	223	YPC 3844.00 (GI 643)
				153.96 ± 4.04	1.2084	222.3	HIP 82809 (GI 643)
Program Stars							
GJ 2005ABC.....	129.47 ± 2.48	0.6537	348.3	135.3 ± 12.1	0.614	355	YPC 66.01
DEN 1048–3956.....	249.78 ± 1.81	1.5388	229.8	247.71 ± 1.55	1.5304	229.2	0.9 m CTIOPI
LTT 6933.....	61.56 ± 1.62	0.9768	196.9	61.11 ± 1.51	0.9593	197.4	0.9 m CTIOPI

^a Identified as LP 658-44.

benefit of reducing the effects of optical distortions on the relative positions of the pi star and the reference stars.

To minimize the effects of differential color refraction (DCR, see § 3.4), a great deal of effort was made to take all parallax frames as close as possible to the meridian. In the case of the brightest targets, the observations were restricted to ±30 minutes from transit, and within that timespan four to six frames were taken. In the case of our faintest program objects (some requiring exposure times as long as 1200 s), they had to be observed within ±60 minutes from the meridian and each time the target was visited only two or three frames could be taken. Exposure times were kept between a minimum of 30 s (to average out transient atmospheric effects) and a maximum of 1200 s (to minimize DCR effects and image distortion caused by imperfect guiding). In some cases the exposure times were determined based on the brightness of the pi star, in others by reference stars brighter than the pi star. In both cases, we always aimed at the highest possible number of counts, restricted of course by the saturation level and by the maximum acceptable exposure time.

Based on previous experience, and given the fine platescale of the CTIO 1.5 m setup, we anticipated that approximately 30 good frames taken over 2 yr would be sufficient to decouple the parallax and proper motion and yield final parallaxes with a precision of about 3 mas. As shown by the results presented in Tables 2 and 3, this was indeed confirmed. Furthermore, under certain ideal conditions it was possible to reach our goal within a shorter time period and with fewer frames. This latter was quite fortunate, because the instrumental setup that was used in the 1.5 m CTIOPI was retired starting in 2003, so it was not possible to complete all parallax series and other observations as we had originally planned.

To check for consistency and detect possible systematic effects, nine parallax calibration stars of the appropriate bright-

ness that are distributed more or less randomly in the sky were observed throughout our program. Results for seven of them are reported here (see Table 3). The results for the remaining two will be discussed in a forthcoming publication (E. Costa et al. 2005, in preparation).

3.2. First Evaluation of the Data

All CCD frames were first calibrated using standard IRAF (ver. 2.11.3, NOAO, University of Arizona)⁵ tasks. For this purpose, zero exposures and dome flats were taken every night.

After sorting all our observations by target, all frames available for a given target were examined, and the best image (in terms of FWHM and signal-to-noise ratio of the pi star) was chosen to perform a reexamination of the preliminary reference frame. In an effort to homogenize the distribution of reference stars, fainter stars were added, increasing the number of reference stars to a maximum of 25. At this point, we definitively confirmed that all of them had a pointlike appearance. In spite of these precautions, in the final reduction it became evident that some of them were not optimum (for a variety of reasons) and had to be rejected.

Using SExtractor (Bertin & Arnouts 1996), we then determined the (X, Y) centroids, the peak flux above background, the ellipticity, and the FWHM of the pi star and reference stars in all images. Given the varied conditions in which the parallax frames were acquired, it was a tricky and time-consuming task to select the appropriate SExtractor search parameters in order to detect the pi star and all reference stars in all images. The results output by SExtractor were then used by a customized program that calculates the parallax factors and takes into

⁵ IRAF is distributed by NOAO, which is operated by AURA, Inc., under cooperative agreement with the NSF.

account DCR effects (see next sections) to select the frames to be kept for the first iteration in the parallax calculation and to select the so-called “trail plate” (see below).

We imposed that, in a given astrometry frame, only reference stars with peak counts between 100 and 65,500, a FWHM smaller than $2''.5$, and an ellipticity less than 0.2 should be kept for the reference system. In a few marginal situations, these constraints were relaxed, and we accepted less than 100 counts and ellipticities as high as 0.6 (but objects were still confirmed to be stellar). For a frame to be useful for parallax calculations, at least five reference stars must meet these criteria. Furthermore, to consider a frame as a trail plate candidate, we imposed that *all* objects of interest should satisfy the above constraints. When more than one image satisfied our requirements, the one with the best FWHM and smallest hour angle was selected as the trail plate. We would like to make clear that these conditions do not apply to the photometric observations (see § 4.1).

3.3. Parallax Factors

In order to calculate the parallax factors, a precise ephemeris of the Earth-to-solar system barycenter distance, as well as good recent epoch coordinates for our targets, is required. The former were obtained from the Jet Propulsion Laboratory (JPL DE405, the best currently available) and the latter from 2MASS. The precision of the 2MASS coordinates is good enough for our purposes ($\sim 0''.1$ in both coordinates), and they have the advantage that they correspond to an observational epoch very similar to that of our survey.

3.4. Differential Color Refraction

Although most of the observations were made near the meridian, thereby minimizing the effects of refraction, we did take a small number of frames with hour angles greater than ~ 1 hr, in which cases DCR cannot be ignored. These latter correspond to exploration and photometry frames taken with the appropriate exposure time and equipment and frames taken for incomplete refraction series, some of which we deemed necessary to include in the reduction of some targets in order to increase the number of frames available.

To check for consistency, our original plan was to determine the DCR correction using both empirical (see, e.g., Monet et al. 1992) and theoretical (see, e.g., Stone 1996) methods as was done in the case of the 0.9 m CTIOPI; this methodology is discussed in detail in J05 and references therein. Both approaches require knowledge of the *VRI* colors of the pi star and of all the parallax reference stars (see § 4), and the empirical methodology also requires ad hoc *VRI* refraction series. Unfortunately, because the 1.5 m CTIOPI program ended before appropriate refraction series could be obtained, we were in principle left with a theoretical solution to DCR as our only option. However, given that the filter sets used in the 0.9 m CTIOPI and 1.5 m CTIOPI are declared as identical, it was expected that the empirical DCR curves of both telescopes would be very similar, so the empirical model derived by J05 was used.

For a few of the targets for which all of the available frames had been taken near culmination, we also calculated their parallaxes without considering DCR. Comparison with calculations including a DCR correction show negligible differences. This confirms the reports by other observers (see, e.g., Dahn et al. 2002) that there is no need for a DCR correction if the observations are restricted to $\pm \sim 20$ minutes from the meridian. On the other hand, tests carried out throughout the 0.9 m CTIOPI using exactly the same DCR model applied here clearly

show the benefits of including a DCR correction if high hour angle frames are used (see J05, Fig. 3).

3.5. Relative Parallaxes

The least-squares astrometric solution of the multiepoch frames taken for each pi star leads to the determination of its parallax and proper motion. This was achieved using a modified version of the University of Texas program GAUSSFIT (Jefferys et al. 1987). More details on the model and the assumptions it uses can be found in J05 and references therein. The procedure requires the selection (as explained above) of one of the frames as trail plate, which defines a fundamental reference system with respect to which all other frames are registered. The true orientation of the trail plate with respect to the International Celestial Reference Frame (Arias et al. 1995) was determined by comparison with the Guide Star Catalog, version 2.2 (GSC2.2, 2001).⁶

In general, GAUSSFIT has to be run several times before a satisfactory parallax result is obtained. After each iteration the output is examined to detect high trigonometric parallax and/or high proper motion reference stars, and the results are further analyzed using IDL⁷ routines to identify high residual frames and high residual reference stars. The offending frames/objects are deleted on a one-by-one basis and GAUSSFIT rerun each time. A high *VRI*-based photometric parallax value (see § 3.6) is also a reason to eliminate a reference star from the final solution.

3.6. Absolute Parallaxes

Because the measured parallax is affected by the distance of the reference star system, to obtain a better estimation of the true parallax (the “absolute parallax”) the results were corrected for this effect. Of the various possible ways to determine this correction (see J05 and references therein for a discussion of the advantages and drawbacks of the three most popular methods), we adopted the photometric parallax method. This method requires the availability of *VRI* photometry (see § 4) for the parallax reference stars and uses previously established relationships between absolute magnitude and color to estimate the distance of the reference stars in each pi star field. The specific relationships between absolute magnitude and color we used were those established between M_v and the colors ($V - R$), ($V - I$), and ($R - I$) by Henry et al. (2004) for dwarfs on the main sequence (using the RECONS database for main-sequence stars). In this approach, the weighted mean photometric parallax of the reference star system represents the correction from relative to absolute parallax (see J05). The mean of the corrections to absolute is 1.31 mas, and the mean error of these corrections is 0.16 mas.

It should be noted that to adopt this procedure we have to assume that all reference stars are main-sequence dwarfs. Because we lack information about the luminosity class of these stars, inevitably there will be some contamination by giants. To evaluate the effect of this contamination, we have run simulations using a model of the Galaxy (described in Mendez & Guzman [1998] and Mendez & van Altena [1996]), which gives the predicted number of stars from different populations as a function of position in the Galaxy, apparent magnitude, and color range. Most of our reference stars are in the range $10 \leq V \leq 19$, while their colors are in the range $0.0 \leq V - I \leq 3.0$. Because our targets are distributed all over the sky, we have

⁶ Space Telescope Science Institute, 2001, The Guide Star Catalogue Version 2.2.01.

⁷ IDL (Interactive Data Language) is a commercial software for data analysis and visualization, developed by Research Systems, Inc., <http://www.rsinc.com>.

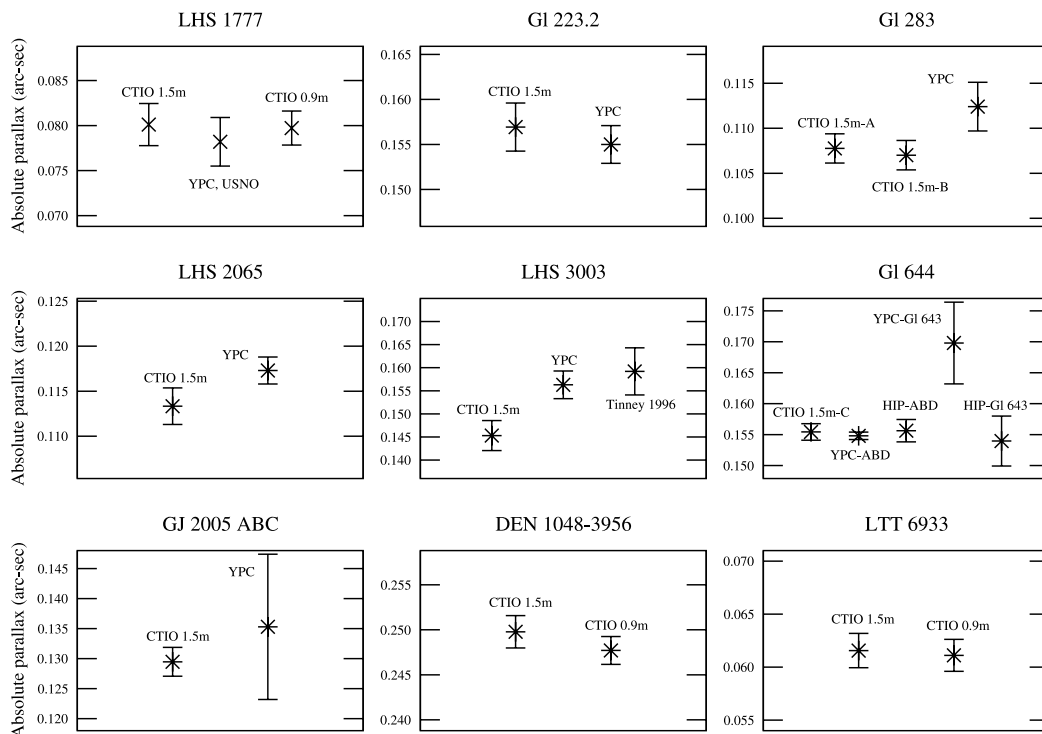


FIG. 1.—Comparison of our 1.5 m CTIOPI parallaxes with published data. See Table 5 and § 3.7 for details. YPC stands for the General Catalogue of Trigonometric Stellar Parallaxes, HIP for the *Hipparcos* and Tycho Catalogues, USNO for the US Naval Observatory, and CTIO 0.9 m for data published by J05. For our parallaxes, error bars are 1σ estimated values as calculated by GAUSSFIT, while those of the comparison results are the published errors.

calculated the plausible range of expected contamination for different combinations of Galactic latitudes and longitudes. We find that, for latitudes $|b| \geq 45^\circ$, the expected contamination is 10% or less. Therefore, for typically 20 reference stars, we would expect 1 to 2 stars to be giants at intermediate and high Galactic latitudes. The net effect of this contamination is to artificially increase the correction from relative to absolute parallax. We estimate that, in this case, the error introduced to the correction would be $\sim 10\%$, which for an overall correction of 1–2 mas (see Table 2) would imply uncertainties of less than 0.2 mas. The worst scenario occurs at very low Galactic latitudes, where the maximum expected contamination is $\sim 20\%$. In this case, the error could be higher but still only of the order of a few tenths of a milliarcsecond. These uncertainties are, however, comparable with the mean error of the photometric parallax method (0.16 mas, given above) and are in all cases much smaller than the typical errors of our final parallaxes. (The mean error of the final parallaxes is 2.48 mas.) We therefore conclude that contamination of our reference frame by giants is not a serious issue, so additional corrections for this effect have not been included. A quick look at Table 2 shows that the final errors are dominated by the relative parallax errors, not by minor errors in the corrections from relative to absolute parallaxes.

3.7. Results and Discussion

Our astrometry results, together with other relevant data, are presented in Table 2. The first column of Table 2 gives the names of the targets, column (2) the relative parallax and its error, column (3) the correction from relative to absolute parallax and its error, column (4) the absolute parallax and its error, column (5) the proper motion and its error, and column (6) the proper-motion position angle and its error. Columns (7), (8), and (9) give the number of parallax frames that were secured for each target, the timespan during which the targets were observed, and the number of independent observing runs in which

they were visited, respectively. Finally, column (10) gives the number of reference stars used in the final reduction process, and column (11) the adopted bandpass.

Table 3 presents a comparison of our results with available parallax and proper-motion data. YPC stands for the General Catalogue of Trigonometric Stellar Parallaxes (van Altena et al. 1995), HIP for the *Hipparcos* and Tycho Catalogues (Perryman 1997), and USNO for the US Naval Observatory (Harrington et al. 1993). It should be noted that while the parallax for LHS 1777 published in YPC is the same as that given in the USNO list and is declared to have been taken directly from Harrington et al., there are slight differences between the proper motion and position angle presented in both works. In Table 3 we have included both sets of results for completeness.

Figure 1, created using the data given in Table 3, illustrates the good agreement between our parallax results and those from other surveys. The largest parallax differences are for LHS 3003 (13.9 mas between our value and the Tinney 1996 value) and for GI 643 (14.4 mas between our value and the YPC value), a distant companion to GI 644C. Both of the reference values have errors larger than 5 mas. In the case of LHS 3003, the YPC value is somewhat intermediate between Tinney’s and ours, while for GI 644C our value is well in accordance with that given by YPC and the *Hipparcos* values for GI 644ABD and GI 643.

The unweighted mean difference $\pi_{1.5\text{ m CTIOPI}} - \pi_{\text{others}}$ over all the comparison stars ($N = 14$, including multiple observations of the same target and independent observations at the 0.9 m telescope within CTIOPI for DEN 1048–3956 and LTT 6933) amounts to -2.88 ± 5.47 mas; i.e., it is zero within the calculated standard deviation, while the mean of the differences $[(\pi_{i,1.5\text{ m CTIOPI}} - \pi_{i,\text{others}})/\sigma_{i,1.5\text{ m CTIOPI}}]$ corresponds to -1.51σ . We therefore conclude that, within the limited number of comparison stars, our results agree quite well with previous determinations.

Particularly important are the comparisons for DEN 1048–3956 and LHS 1777. Both of our parallax values were obtained

TABLE 4
OPTICAL PHOTOMETRY

Name (1)	V (2)	R (3)	I (4)	σ_V (5)	σ_R (6)	σ_I (7)	N_{obs} (8)
GJ 2005ABC.....	15.338	13.502	11.403	0.040	0.046	0.035	8
LHS 132.....	18.575	16.223	13.793	0.056	0.016	0.005	4
LP 647-013.....	19.266	17.168	14.708	0.116	0.060	0.039	6
LHS 148.....	16.411	15.431	14.553	0.013	0.012	0.008	14
WT 84.....	15.674	14.185	12.246	0.004	0.008	0.005	4
LHS 162.....	15.358	14.352	13.337	0.008	0.004	0.008	20
LP 412-031.....	18.881	16.904	14.484	0.101	0.023	0.004	4
WT 133.....	16.030	14.665	12.962	0.012	0.003	0.008	8
APMPM J0425–7243.....	15.918	14.591	12.860	0.030	0.011	0.007	4
APMPM J0452–5819.....	18.507	16.429	14.136	0.038	0.028	0.057	4
LHS 1777.....	15.358	13.838	11.971	0.002	0.009	0.007	6
GI 223.2.....	14.497	13.994	13.538	0.003	0.003	0.004	4
CE 426–023.....	17.439	16.161	14.481	0.019	0.007	0.011	4
WT 214.....	16.061	14.799	13.141	0.029	0.011	0.015	12
GI 283B.....	16.696	14.695	12.370	0.019	0.003	0.002	8
GI 283A.....	13.061	12.886	12.728	0.002	0.002	0.003	2
WT 233.....	16.225	15.324	14.422	0.035	0.019	0.015	4
LHS 2065.....	18.959	16.781	14.487	0.176	0.044	0.041	4
DEN 1048–3956.....	17.532	15.051	12.543	0.057	0.014	0.047	6
CE 440–064.....	16.349	14.849	12.937	0.022	0.007	0.007	4
LHS 367.....	13.246	12.343	11.521	0.009	0.013	0.018	10
LHS 3003.....	17.141	14.865	12.507	0.036	0.045	0.054	10
SPM 57600401.....	15.258	13.997	12.376	0.030	0.027	0.096	10
GI 644C.....	16.916	14.566	12.196	0.057	0.012	0.015	14
LTT 6933.....	12.799	11.523	9.950	0.004	0.010	0.009	10
LHS 3346.....	15.152	13.909	12.425	0.031	0.008	0.010	10
WT 2180.....	16.644	14.968	13.036	0.011	0.007	0.010	6
APMPM J1957–4216.....	18.099	16.402	14.312	0.051	0.036	0.039	10
LTT 7944.....	14.883	13.802	12.513	0.010	0.012	0.007	12
LHS 3566.....	17.618	15.666	13.638	0.068	0.034	0.055	12
APMPM J2204–3348.....	15.464	14.427	13.440	0.010	0.016	0.011	8

in marginal conditions (LHS 1777 to a lesser extent) in terms of the number of parallax frames that were secured, the timespan during which they were observed, and the number of independent observing runs in which they were visited (see Table 2); yet, our results agree well within the declared errors with those from the 0.9 m CTIOPI. This unexpected success can probably be explained by the fine scale of the CTIO 1.5 m setup and by the good reference frames that could be established around these targets.

3.8. Notes on Individual Fields

Here we comment on situations that may have affected the quality of the astrometry. “Inhomogeneous reference frame” refers to a situation in which all the reference stars are located on one side of the pi star field. (Finders can be found in the RECONS Web site.) We arbitrarily catalog as “sparse” any reference frame with less than 15 reference stars.

GJ 2005.—Inhomogeneous and sparse reference frame. Observed at V to suppress companions at $\sim 1''$ to the north.

LHS 148.—Sparse reference frame.

WT 84.—Sparse reference frame. Various faint, blended companions noticeable only in very good seeing frames. With the present material it is not possible to confirm whether the companions are physical or optical.

LHS 162.—Sparse reference frame.

WT 133.—Sparse reference frame. Also, as indicated by their trigonometric distances, the reference system used in

the final reduction seems to include various nearby stars ($\pi \geq 5$ mas).

APMPM J0425–7243.—Sparse reference frame. Faint, blended companion to the northwest, noticeable only in very good seeing frames. With the present material it is not possible to confirm whether it is a physical or an optical companion. Relatively bright, partially blended companion to the northeast. It *seems* to be an optical companion.

LTT 6933.—Inhomogeneous reference frame.

LHS 3346.—Faint, blended companion to the southeast; detectable only in the best seeing frames. With the present material it is not possible to confirm whether it is a physical or an optical companion.

APMPM J1957–4216.—Variability suspected. In early frames this object is clearly brighter. Furthermore, its photometric errors (see Table 4) are relatively high; this is in spite of the fact that the star is bright and that all the photometric data is of good quality.

4. THE PHOTOMETRY

4.1. Observations and Reductions

Our pipeline requires knowledge of the VRI colors of the targets and the parallax reference stars in their fields to address DCR and the correction from relative to absolute parallax.

Looking for homogeneity, we originally planned to carry out the photometric observations of the 1.5 m CTIOPI targets with exactly the same setup used to make their parallax

observations. However, it soon became evident that, given the relatively large number of targets and the enormous amount of time that was required to obtain adequate photometry of our faintest objects (not to mention the nights lost because of bad weather), a strategy focused on homogeneity would not be possible. It was necessary therefore to use a variety of telescopes to fulfill our needs; namely, the Danish 1.54 m telescope at La Silla (ESO), the 1.5 and 0.9 m telescopes at CTIO, and the 1.0 m telescope at LCO. Inevitably, our *VRI* instrumental photometric system varied from one observatory to another, but care was taken to choose from whatever sets of filters were available at each site those known to reproduce the standard *VRI* Johnson-Kron-Cousins system best. Comparison of results obtained with all four setups indeed do not show obvious systematic effects that could be of importance for the above purposes. An EEV/MAT 2048×4096 CCD with Bessell *VR* and Gunn *i* filters was used at ESO, a Tektronic 2048×2046 CCDs with Tek filters at both the CTIO 0.9 and 1.5 m telescopes, and a SITe 2048×3150 CCD with Harris filters at LCO. Care was taken to operate all detectors well within the linear range of their response.

Typically, six *UBVRI* standard star areas from the catalogs of Landolt (1992) and Graham (1982) were observed multiple times each night to determine the transformation of our instrumental magnitudes to the standard *VRI* system. Although most of these areas include stars of a wide variety of colors, given the very red colors of many of our targets very red standards (also from the Landolt catalogue) were also observed. A few of the standard areas were followed each night up to about 2.2 air masses to determine atmospheric extinction optimally. All program stars were observed during transit, following the sequence *VRIIRV*. Although time consuming, this latter practice has proved very useful to check for consistency.

The CCD frames were first calibrated using standard IRAF tasks. For this purpose, zero exposures and twilight sky flats were taken every night. Aperture photometry was then performed on each object of interest using the IRAF APPHOT package. (A special procedure was used in the case of targets with close companions—see below.) The optimum aperture size for each night, ensuring a negligible loss of light from the point-spread function (PSF) wings and minimizing light contamination from close objects, was determined by means of the IRAF MKAPFILE task. The best aperture radius turned out to be 4–5 times the average FWHM of the frames.

To put our observations into the standard system, we used the transformation equations

$$\begin{aligned} v &= V + v_1 + v_2 X_v + v_3(V - R) + v_4(V - R)X_v, \\ r &= R + r_1 + r_2 X_r + r_3(V - R) + r_4(V - R)X_r, \\ i &= I + i_1 + i_2 X_i + i_3(V - I) + i_4(V - I)X_i, \end{aligned} \quad (1)$$

where (v , r , and i) and (V , R , and I) are the instrumental and standard magnitudes respectively, (X_v , X_r , and X_i) are the air masses, and v_1 , v_2 , v_3 , v_4 , etc., are constants. It should be noted that, in the absence of blue passband observations, it was not possible to use (as is the common practice) the ($B - V$) color for the standardization of the v magnitude. However, as shown by Bucciarelli et al. (2001), the ($B - V$) and ($V - R$) colors of the Landolt stars are linearly related and comparable in range, so the use of the ($V - R$) color in the (v , V) equation is equally satisfactory.

Equations (1) were applied to the Landolt/Graham standard star magnitudes and solved using the IRAF FITPARAMS task,

which performs a least-squares fit to the system. This task can be run interactively, permitting the rejection of problematic observations to control the quality of the fit. Without major intervention, the rms of all fits turned out to be about 0.02 mag. In most cases, the formal errors of the calculated coefficients were significantly smaller than their derived values.

Finally, the above set of transformation equations with their corresponding calculated coefficients was applied to our program stars for their calibration. This was done by means of the IRAF INVERTFIT task, which produces a set of calibrated magnitudes and colors together with their corresponding errors: V , error(V); ($V - R$), error($V - R$); and ($V - I$), error($V - I$). With the exception of Gl 283A, for which only one photometric observation is available, the IRAF-computed errors were not used because, as pointed out by Bucciarelli et al. (2001), the final photometric error computed by INVERTFIT does not rigorously treat error propagation, therefore producing a lower limit of the photometric errors.

A few targets turned out to have stars close enough to be included in the ideal aperture chosen to do the photometry, thereby contaminating the instrumental magnitudes. In the case of faint contaminating stars that are not too close to the target, they were simply removed using the IRAF IMEDIT task, which replaces the offending object with an average sky value determined from nearby sky pixels. In those cases in which the contamination was serious (bright, relatively close stars), a more elaborate procedure was necessary, combining aperture photometry and PSF photometry the latter made using the IRAF DAOPHOT package. In this procedure, we first select a set of 6 to 8 comparison stars in the vicinity of the contaminated target, of similar brightness to the target, and free of close stars. We then carry out both aperture and PSF photometry of the target and the comparison stars, choosing the PSF parameters so as to fit the target's PSF core, excluding the contaminating object. In this way, we produce two sets of instrumental magnitudes: apertures and PSFs. In the cases of the comparison stars, the differences between these values are then averaged by passband to obtain the corrections to be applied to the target's PSF magnitudes. (This would be equivalent to applying a standard aperture correction.) It should be noted that in the case of very close faint stars, it was not possible to remove them, but given the brightness difference with the targets, their effect is negligible.

4.2. Results

The results of our *VRI* photometry for the pi stars are presented in Table 4. The first column gives the name of the targets; columns (2), (3), and (4) their average *VRI* magnitudes (we give magnitudes instead of colors mainly for comparison purposes—they were obtained directly from the IRAF output); and columns (5), (6), and (7) the corresponding standard deviation for all cases with at least three independent measurements. These errors have to be interpreted with caution; it must be kept in mind that they have been derived from a small number of independent observations and, furthermore, that some of our targets could be variable. Finally, column (8) gives the number of times the star was observed. We do not present the *VRI* photometry of the parallax reference stars here, but it is available on request.

In Table 5, we give the *IJK_s* infrared data available for our targets, extracted from the 2MASS and the Deep Near Infrared Survey of the Southern Sky (DENIS), together with the corresponding 2MASS and DENIS identifications. Part of this imported data was used for comparison purposes and to construct color-magnitude and color-color diagrams (CMDs and CoCoDs, respectively; see § 5); the rest is included for completeness.

TABLE 5
INFRARED PHOTOMETRY FROM 2MASS AND DENIS

Name	2MASS							DENIS						
	ID	J	Err $_J$	H	Err $_H$	K_s	Err $_K$	ID	I	Err $_I$	J	Err $_J$	K_s	Err $_K$
GJ 2005ABC.....	00244419–2708242	9.254	0.034	8.547	0.036	8.241	0.030
LHS 132.....	01025100–3737438	11.130	0.023	10.479	0.024	10.069	0.021
LP 647-013.....	01095117–0343264	11.694	0.021	10.931	0.026	10.428	0.025	J010951.1–034326	14.820	0.060	11.609	0.080	10.260	0.100
LHS 148.....	01530890–3325022	13.519	0.029	13.012	0.030	12.832	0.032	J015308.9–332502	14.508	0.050	13.542	0.090	12.880	0.150
WT 84.....	02172845–5922435	10.438	0.026	9.868	0.021	9.542	0.019	J021728.3–592243	12.291	0.040	10.452	0.060	9.511	0.060
LHS 162.....	02561319–3508265	12.280	0.026	11.725	0.024	11.536	0.021
LP 412-31.....	03205965+1854233	11.759	0.021	11.066	0.022	10.639	0.018
WT 133.....	04021391–4325264	11.290	0.023	10.715	0.024	10.452	0.021	J040213.8–432526	12.911	0.040	11.392	0.080	10.508	0.080
APMPM J0425–7243.....	04243351–7243055	11.214	0.022	10.674	0.023	10.402	0.021
APMPM J0452–5819.....	04513734–5818519	11.691	0.024	11.089	0.023	10.705	0.023
LHS 1777.....	05421271–0527567	10.206	0.023	9.694	0.023	9.371	0.019
GI 223.2.....	05550948–0410042	13.047	0.027	12.860	0.027	12.777	0.026
CE 426-023.....	06224496–2816526	12.909	0.023	12.482	0.027	12.212	0.025
WT 214.....	07284011–6120413	11.611	0.023	11.106	0.025	10.860	0.023	J072840.0–612041	13.145	0.030	11.625	0.060	10.800	0.070
GI 283B.....	07401922–1724449	10.155	0.022	9.628	0.023	9.291	0.021
GI 283A.....	07402064–1724481	12.653	0.022	12.611	0.026	12.583	0.036
WT 233.....	07561341–6705205	13.374	0.024	12.870	0.023	12.627	0.024
LHS 2065.....	08533619–0329321	11.212	0.026	10.469	0.026	9.942	0.024
DEN 1048–3956.....	10481463–3956062	9.538	0.022	8.905	0.044	8.447	0.023	J104814.4–395608	12.637	0.030	9.640	0.070	8.507	0.070
CE 440-064.....	11485053–2833230	11.131	0.022	10.636	0.022	10.347	0.019	J114850.5–283323	12.892	0.020	11.091	0.050	10.304	0.080
LHS 367.....	14182047–5224123	10.500	0.023	9.981	0.022	9.786	0.019	J141820.3–522412	11.514	0.020	10.653	0.070	9.781	0.070
LHS 3003.....	14563831–2809473	9.965	0.026	9.315	0.022	8.928	0.027
SPM 57600401.....	16131715–2538139	10.964	0.024	10.461	0.023	10.177	0.021	J161317.2–253813	12.337	0.040	10.942	0.070	10.154	0.070
GI 644C.....	16553529–0823401	9.776	0.029	9.201	0.024	8.816	0.023
LTT 6933.....	17280732–6227145	8.422	0.023	7.847	0.059	7.567	0.017
LHS 3346.....	17584996–5605412	10.893	0.022	10.281	0.025	10.000	0.019
WT 2180.....	19482268–0822520	11.120	0.026	10.541	0.021	10.191	0.021	J194822.6–082252	12.990	0.030	11.043	0.060	10.261	0.060
APMPM J1957–4216.....	19565761–4216235	12.383	0.022	11.995	0.022	11.661	0.028	J195657.5–421622	14.336	0.030	12.268	0.070	11.658	0.090
LTT 7944.....	20071538–5421489	11.240	0.024	10.775	0.027	10.520	0.021
LHS 3566.....	20392378–2926335	11.357	0.025	10.743	0.023	10.367	0.022
APMPM J2204–3348.....	22040227–3347383	12.324	0.027	11.807	0.029	11.601	0.027	J220402.3–334739	13.355	0.040	12.409	0.090	11.630	0.120

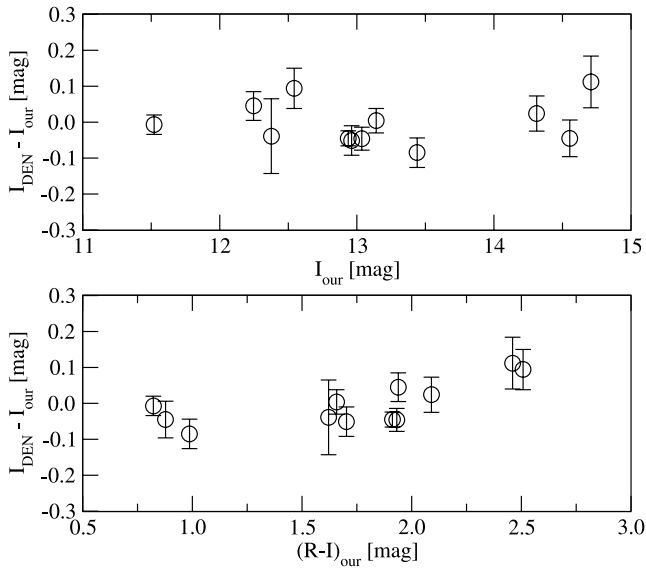


FIG. 2.—Comparison of our Kron-Cousins RI photometry with DENIS Gunn i photometry. The error bars represent the square root of the DENIS error and our error added in quadrature.

Figure 2 shows the good agreement existing between our Kron-Cousins I -band photometry (I_{our}) and Gunn i DENIS (I_{DEN}) observations. For the 12 objects in common, we obtain: $\langle I_{\text{DEN}} - I_{\text{our}} \rangle = -0.003 \pm 0.037$ mag. The error bars represent the square root of the DENIS error and our error added in quadrature. There is no obvious dependence with I , but a small trend with $(R - I)$ is suggested. To further check for consistency, we made a comparison between the 2MASS and DENIS J -band and K_s -band photometry for these 12 stars. We obtained $\langle J_{\text{DEN}} - J_{2\text{MASS}} \rangle = 0.051 \pm 0.013$ mag and $\langle K_{\text{DEN}} - K_{2\text{MASS}} \rangle = -0.006 \pm 0.040$ mag. No magnitude or color systematic trends were detected. This is in good agreement with the more detailed comparisons between the DENIS and 2MASS photometry done by Carpenter (2001) and Cabrera-Lavers & Garzón (2003).

5. COLOR-MAGNITUDE AND COLOR-COLOR DIAGRAMS

In this section we present selected CMDs and CoCoDs that, in combination with theoretical isochrones from the literature and other derived properties of the observed sample, have aided to identify the general nature of each of our targets.

In Figure 3 we present two CMDs: an M_R versus $R - I$ CMD constructed with RI data from the present survey and an M_J versus $I - J$ CMD constructed combining our I -band data with J -band data from 2MASS. Other magnitude-color combinations tested did not show significant differences. The absolute magnitudes M_R and M_J and their associated errors, σ_{M_R} and σ_{M_J} , were computed from the usual expressions,

$$M = m + 5 \log_{10} \pi + 5, \quad (2)$$

$$\sigma_M = \sqrt{\sigma_m^2 + \left(\frac{\sigma_\pi}{0.2 \ln 10 \pi} \right)^2}, \quad (3)$$

where π and σ_π are the parallax and its estimated uncertainty in arcseconds for an object of apparent magnitude and error $m \pm \sigma_m$. The color error bars represent the square root of the corresponding magnitude errors added in quadrature.

For interpretation purposes, we have superposed various theoretical isochrones on our CMDs in Figure 3. We present two sets of solar metallicity ($Z = 0.019$, $[\text{Fe}/\text{H}] = 0$) isochrones for very low mass stars (VLMs) and brown dwarfs (BDs) from models by Chabrier et al. (2000). The thin solid line is for 0.1 Gyr objects (VLM + BD in Fig. 3) and the dotted line for 5.0 Gyr objects (VLM in Fig. 3). Both sets of models were computed for masses below $0.1 M_\odot$. The transition between VLMs and BDs in these models occurs for a mass of $\sim 0.07 M_\odot$.

We also present isochrones for 4.5 Gyr solar metallicity red dwarfs (RDs), from models by Baraffe et al. (1998; *thick solid lines*). These isochrones also extend to very low masses, but, in order to avoid misleading comparisons with the VLM/BD isochrones, in Figure 3 we have plotted them only to a lower mass limit of $0.1 M_\odot$. The motive for this was that, although both sets of isochrones are from the same group of authors, they are not strictly comparable because of differences in the physics of the models. The models by Chabrier et al. (2000) are supposed to supersede those by Baraffe et al. (1998). To illustrate the effect of age and metallicity on the Baraffe et al. (1998) RD isochrones, we have also superposed a 10 Myr solar metallicity RD isochrone (*dot-dashed line*) and a 4.5 Gyr Population II abundance RD isochrone (*dashed line*). Numbers for individual stars in Figure 3 (and also in Figs. 4 and 5; see below) are those from Table 1.

In the CMDs, the fainter half of our points, including our three latest spectral type targets, LP 647-013 (No. 3), LHS 2065 (No. 18), and DEN 1048-3956 (No. 19), are consistent with the 0.1 Gyr VLM + BD isochrone. This seems to imply that we have a large sample of BDs. However, it should be kept in mind that such a straightforward interpretation must be taken with caution. It is difficult from CMDs alone to distinguish young BDs from solar-age VLMs. If the isochrones shown for 5.0 Gyr VLMs are systematically too faint, then most of our targets would be normal stars, as we suspect. It is, of course, also possible that the photometry may be affected by unknown systematic effects. Note that from the Chabrier et al. (2000) models, the most massive BDs ($0.07 M_\odot$) have $M_R \sim 13.6$ and $M_J \sim 9.8$ at age 0.1 Gyr. The same massive BDs fade to $M_R \sim 22.1$ and $M_J \sim 15.2$ at 5.0 Gyr (beyond the limits of our plots). Finally, the parallax calibration star LHS 2065 is a known flare star, so its slightly deviant position in the M_R versus $R - I$ CMD could be explained if it was observed during a flare while the VRI photometry was secured.

With the possible exception of a few objects, our CMDs show no unusual features in the RD regime. Abundance and/or age variations can explain well the overall dispersion around the RD 4.5 Gyr solar metallicity isochrone. Of the six stars that lie more or less clearly below the RD main sequence, in the Population II domain—LHS 148 (No. 4), LHS 162 (No. 6), WT 233 (No. 17), LHS 367 (No. 21), LTT 7944 (No. 29), and APMPM J2204-3348 (No. 31)—five have been spectroscopically identified as subdwarfs by L05 and/or B05: LHS 148, LHS 162, WT 233, LHS 367, and APMPM J2204-3348. All of them have the distinctive $\text{Ca}Hn$ ($n = 1-3$) features of red subdwarfs from 6345 to 7000 Å. Furthermore, a look at Table 6, which gives tangential velocities (V_{tan}) for all our targets—along with other derived properties, including their distances and their M_R and M_J absolute magnitudes—shows that all have high V_{tan} , which is consistent with their spectroscopic classification. They will be further discussed in upcoming spectroscopy papers.

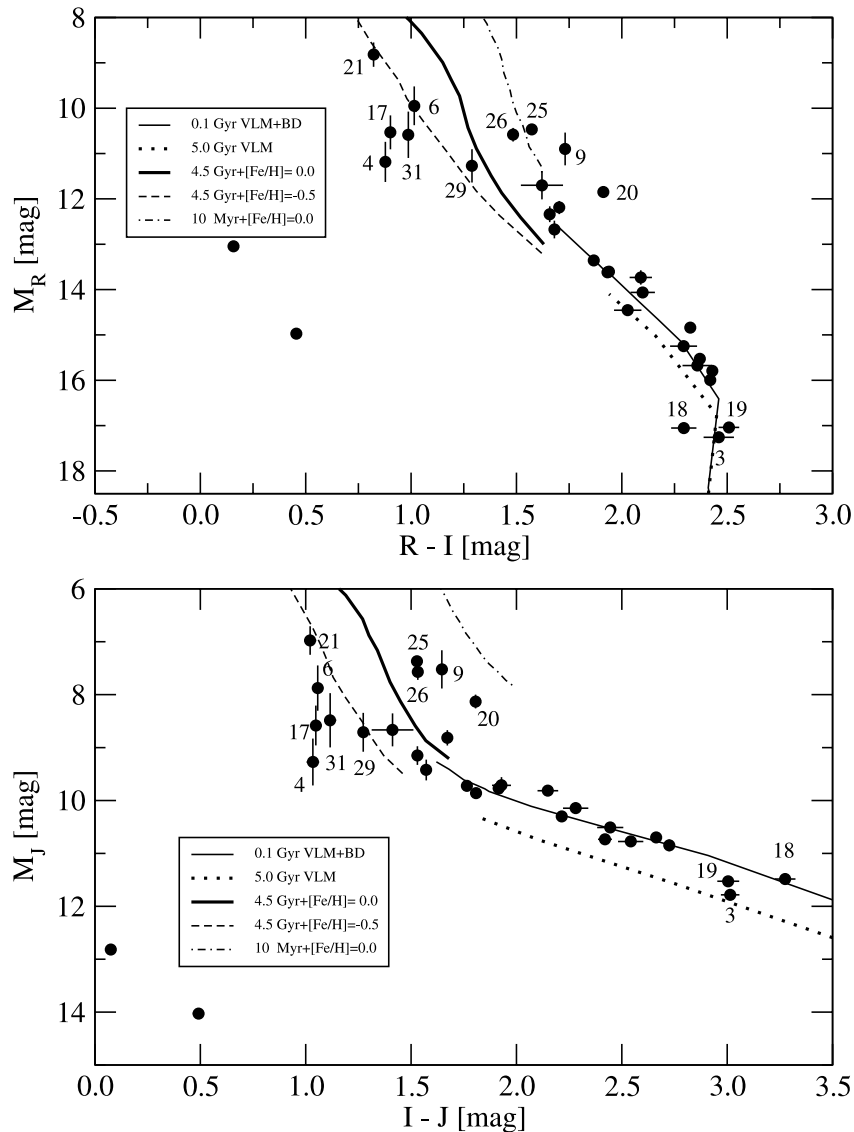


FIG. 3.—Selected CMDs. The top diagram is based on RI data obtained in the present survey. The bottom diagram combines I -band data from our survey with J -band data from 2MASS. We have superposed two sets of solar metallicity ($Z = 0.019$, $[\text{Fe}/\text{H}] = 0$) isochrones for very low mass stars and brown dwarfs, from models by Chabrier et al. (2000). The thin solid line is for 0.1 Gyr objects (VLM + BD), and the dotted line is for 5.0 Gyr objects (VLM). We also present isochrones for 4.5 Gyr solar metallicity, 10 Myr solar metallicity, and 4.5 Gyr Population II abundance red dwarfs (*thick solid lines, dot-dashed lines, and dashed lines, respectively*), all from models by Baraffe et al. (1998). See text for details. The numbers on points correspond to those given in Table 1. Stars labeled are discussed in the text. The two white dwarfs that stand out are the parallax calibration stars Gl 223.2 and Gl 283A.

In Figure 4 we present a M_{K_s} versus $V - K_s$ CMD, constructed combining data from various sources, that illustrates the position of our targets (*circles*) in relation to the RECONS sample of nearby stars (*asterisks*; Henry et al. 2004) and to the Gizis & Reid (1997) sample of subdwarfs with $\mu \geq 1'' \text{ yr}^{-1}$ (*squares*). The line included is an empirical fit tracing the main sequence. A quick look at this figure shows that the six objects that lie below the RD main sequence in our CMDs are in the subdwarf domain (defined by the Gizis & Reid sample). This suggests that LTT 7944 (No. 29) could be a mild subdwarf, in spite of the fact that our spectrum indicates it is a M3.0 V star and its rather low V_{tan} (85.9 km s^{-1}). Further observations are required to settle this interesting discrepancy. It should be noted that the two white dwarfs that stand out in Figure 3 (the parallax calibration stars Gl 223.2 and Gl 283A) have not been included in Figure 4.

In Figure 5 we present a CoCoD constructed combining our RI data with J -band data from 2MASS. (Other color-color com-

binations we tested did not show significant differences.) For completeness we have superposed isochrones with the same properties as those used in the CMDs. Perhaps the most interesting feature in our CoCoD is the fact that the five confirmed subdwarfs discussed in the above paragraphs stand out clearly, forming a compact group. The suspected subdwarf (LTT 7944), however, lies quite separate from this group. As was the case in our CMDs, being a flare star the position of LHS 2065 (No. 18) could be explained as we did in the case of our CMD.

Finally, we would like to comment on four objects, APM 216 (No. 9), CE 440-064 (No. 20), LTT 6933 (No. 25), and LHS 3346 (No. 26), which lie clearly above the mean locus for low-mass main-sequence stars (see Figs. 3 and 4). Although their position could be a consequence of the natural spread in metallicity for disk stars and/or possible multiplicity effects, an interesting possibility is that they could actually be pre-main-sequence stars, such as those found in nearby star-forming regions by, e.g., Torres et al. (2000).

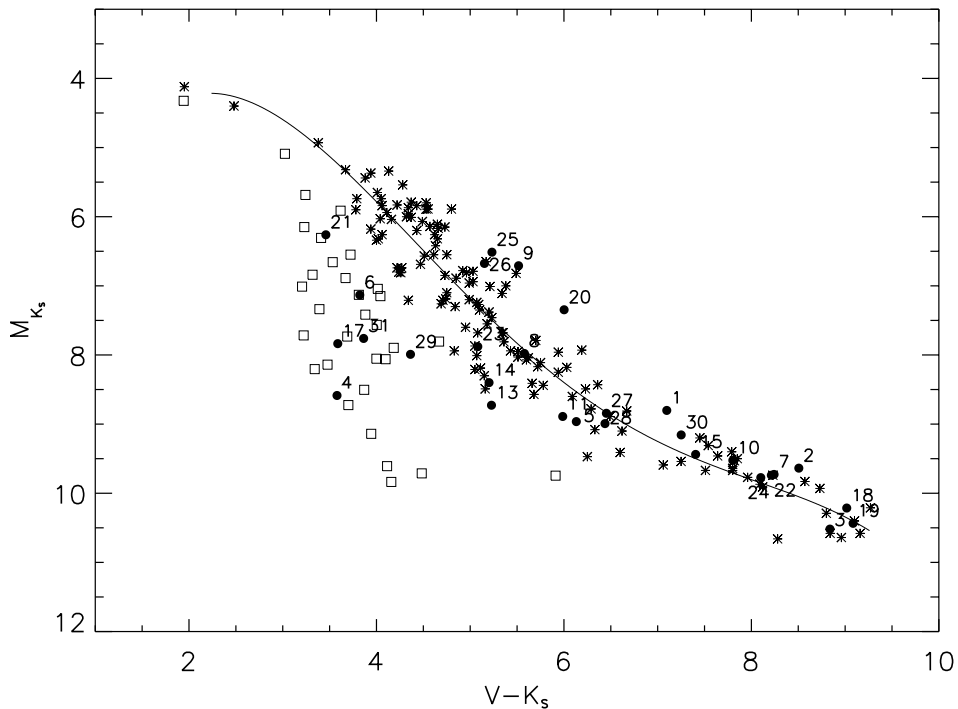


FIG. 4.— M_{K_s} vs. $V - K_s$ CMD, constructed combining data from various sources, which illustrates the position of all our targets (circles) in relation to the RECONS sample of nearby stars (asterisks; Henry et al. 2004) and to the Gizis & Reid (1997) sample of subdwarfs with $\mu \geq 1^{\circ}0 \text{ yr}^{-1}$ (squares). The line included is an empirical fit tracing the main sequence. The numbers beside the circles are those given in Table 1. It should be noted that the two white dwarfs that stand out in Fig. 3 have not been included in this figure.

TABLE 6
DERIVED PROPERTIES FOR THE OBSERVED SAMPLE

Name	Distance (pc)	V_{tan} (km s^{-1})	M_R (mag)	M_J (mag)
GJ 2005ABC.....	7.7	23.9	14.1	9.8
LHS 132.....	12.2	85.6	15.8	10.7
LP 647-013.....	9.6	16.4	17.3	11.8
LHS 148.....	70.7	357.6	11.2	9.3
WT 84.....	13.1	32.9	13.6	9.9
LHS 162.....	76.0	366.1	9.9	7.9
LP 412-31.....	15.2	30.7	16.0	10.8
WT 133.....	31.2	85.9	12.2	8.8
APMPM J0425–7243.....	54.8	133.0	10.9	7.5
APMPM J0452–5819.....	17.2	58.9	15.2	10.5
LHS 1777.....	12.5	57.3	13.4	9.7
GI 223.2.....	6.4	71.5	15.0	14.0
CE 426-023.....	49.8	48.7	12.7	9.4
WT 214.....	31.0	92.3	12.3	9.2
GI 283B.....	9.3	56.3	14.8	10.3
GI 283A.....	9.3	55.5	13.0	12.8
WT 233.....	90.8	326.5	10.5	8.6
LHS 2065.....	8.8	23.1	17.1	11.5
DEN 1048–3956.....	4.0	29.2	17.0	11.5
CE 440-064.....	39.8	127.0	11.8	8.1
LHS 367.....	50.7	273.9	8.8	7.0
LHS 3003.....	6.9	31.8	15.7	10.8
SPM 57600401.....	28.8	50.7	11.7	8.7
GI 644C.....	6.4	36.2	15.5	10.7
LTT 6933.....	16.2	75.2	10.5	7.4
LHS 3346.....	46.2	155.6	10.6	7.6
WT 2180.....	18.6	48.5	13.6	9.8
APMPM J1957–4216.....	34.2	166.3	13.7	9.7
LTT 7944.....	32.1	85.9	11.3	8.7
LHS 3566.....	17.5	66.2	14.5	10.1
APMPM J2204–3348.....	58.6	272.1	10.6	8.5

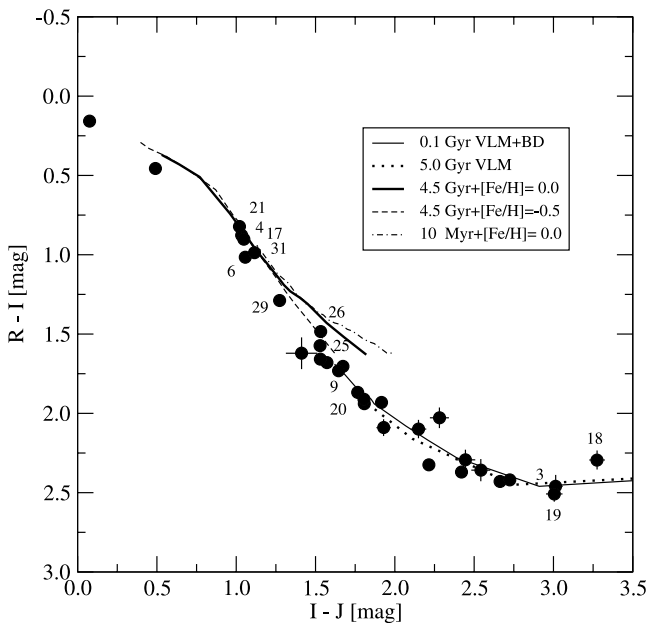


FIG. 5.—CoCoD constructed combining RI data obtained in the present survey with J -band data from 2MASS. For completeness, we have superposed isochrones with the same properties as those plotted in the CMDs. The numbers on the points correspond to those given in Table 1. Stars labeled are discussed in the text.

6. CONCLUSIONS

We summarize here the main conclusions of this work.

1. We present 31 final parallaxes from the 1.5 m CTIOPI program. Twenty-four are of nearby star candidates, and seven are of parallax calibration stars. We provide the first parallaxes for 21 stellar systems. We also provide additional measurements of the new nearby stars DEN 1048–3956 and LTT 6933 and give an improved parallax for GJ 2005, an important low-mass triple system discussed by Leinert et al. (2001).
2. Within the limited number of comparison stars (seven), our results agree well with other parallax determinations.
3. Of the 21 systems with first parallaxes reported here, one is within 10 pc (LP 647-013) and six additional systems are between 10 and 25 pc, the classical distance limit of the Catalog of Nearby Stars and the NStars project.
4. Three of the objects targeted by the present survey, DEN 1048–3956, GJ 2005, and LP 647-013, lie at distances less than 10 pc, the horizon of the Research Consortium on Nearby Stars. They are promising objects for upcoming extra solar planetary searches from space, such as the *Space Interferometry Mission* and the *Terrestrial Planet Finder* mission.
5. Our color-magnitude and color-color diagrams, in combination with theoretical isochrones, have aided the identification of the nature of most of our targets. We have in this way discovered five new subdwarfs (APMPM J2204–3348, LHS 148, LHS 162, LHS 367, and WT 233) and several very low mass (possibly brown dwarf) stars.
6. Our results directly contribute to improving the colors and luminosities of the lower main-sequence stars and to the quest

of completing the nearby star census. By expanding the database for the solar neighborhood stars, they will also contribute to investigations of the luminosity function, mass function, and kinematics of the stars in the vicinity of our sun.

E. C. and R. A. M. acknowledge support by the Fondo Nacional de Investigación Científica y Tecnológica (proyecto No. 1010137, FONDECYT) and by the Chilean Centro de Astrofísica FONDAP (15010003). This project has made generous use of the 10% Chilean time. We thank Gaspare Lo Curto for his assistance in determining the spectral types given here, in advance of publication. The RECONS team at Georgia State University (GSU) is supported by NASA's *Space Interferometry Mission* and GSU. This work has used data products from the 2MASS, which is a joint project of the University of Massachusetts and the Infrared Processing and Analysis Center at the California Institute of Technology funded by NASA and the NSF. This work also used data products from DENIS, which is the result of a joint effort involving several institutes, mostly located in Europe. They are supported mainly by the French Institut National des Sciences de l'Univers, CNRS, and the French Education Ministry; the European Southern Observatory, the State of Baden-Wuerttemberg, and the European Commission under the SCIENCE and Human Capital and Mobility programs; the Landessternwarte, Heidelberg, l'Institut d'Astrophysique de Paris, the Institut für Astrophysik der Universität Innsbruck, and Instituto de Astrofísica de Canarias. The early phase of CTIOPI was supported by the NStars project through the NASA Ames Research Center.

REFERENCES

- Arias, E. F., Charlot, P., Feissel, M., & Lestrade, J.-F. 1995, *A&A*, 303, 604
 Baraffe, I., Chabrier, G., Allard, F., & Hauschildt, P. H. 1998, *A&A*, 337, 403
 Bertin, E., & Arnouts, S. 1996, *A&AS*, 117, 393
 Bucciarelli, B., et al. 2001, *A&A*, 368, 335
 Cabrera-Lavers, A., & Garzón, F. 2003, *A&A*, 403, 383
 Carpenter, J. M. 2001, *AJ*, 121, 2851
 Chabrier, G., Baraffe, I., Allard, F., & Hauschildt, P. 2000, *ApJ*, 542, 464
 Dahn, C. C., et al. 2002, *AJ*, 124, 1170
 Gizis, J. E., & Reid, I. N. 1997, *PASP*, 109, 849
 Graham, J. A. 1982, *PASP*, 94, 244
 Harrington, R. S., et al. 1993, *AJ*, 105, 1571
 Henry, T. J., Ianna, P. A., Kirkpatrick, J. D., & Jahreiss, H. 1997, *AJ*, 114, 388
 Henry, T. J., Subasavage, J. P., Brown, M. A., Beaulieu, T. D., Jao, W., & Hambly, N. C. 2004, *AJ*, 128, 2460
 Henry, T. J., Walkowicz, L. M., Barto, T. C., & Golimowski, D. A. 2002, *AJ*, 123, 2002
 Jao, W.-C., Henry, T. J., Subasavage, J. P., Bean, J. L., Costa, E., Ianna, P. A., & Méndez, R. A. 2003, *AJ*, 125, 332
 Jao, W.-C., Henry, T. J., Subasavage, J. P., Brown, M. A., Ianna, P. A., Bartlett, J. L., Costa, E., & Méndez, R. A. 2005, *AJ*, 129, 1954
 Jefferys, W. H., Fitzpatrick, M. J., & McArthur, B. E. 1987, *Celest. Mech.*, 41, 39
 Landolt, A. U. 1992, *AJ*, 104, 340
 Leinert, C., Jahreiss, H., Woitas, J., Zucker, S., Mazeh, T., Eckart, A., & Köhler, R. 2001, *A&A*, 367, 183
 Méndez, R. A., & Guzman, R. 1998, *A&A*, 333, 106
 Méndez, R. A., & van Altena, W. F. 1996, *AJ*, 112, 655
 Monet, D. G., Dahn, C. C., Vrba, F. J., Harris, H. C., Pier, J. R., Luginbuhl, C. B., & Ables, H. D. 1992, *AJ*, 103, 638
 Perryman, M. A. C. 1997, *The Hipparcos and Tycho Catalogues* (ESA SP-1200; Noordwijk: ESA)
 Stone, R. C. 1996, *PASP*, 108, 1051
 Tinney, C. G. 1996, *MNRAS*, 281, 644
 Torres, C. A. O., da Silva, L., Quast, G. R., de la Reza, R., & Jilinski, E. 2000, *AJ*, 120, 1410
 van Altena, W. F., Lee, J. T., & Hoffleit, E. D. 1995, *The General Catalogue of Trigonometric (Stellar) Parallaxes* (4th ed.; New Haven: Yale Univ. Obs.)